optica

Two-dimensional topological quantum walks in the momentum space of structured light

Alessio D'Errico,[1,†] Filippo Cardano,[1,8,†] Maria Maffei,[1,2] Alexandre Dauphin,[2,6] Raouf Barboza,[1] Chiara Esposito,[1] Bruno Piccirillo,[1] Maciej Lewenstein,[2,3] Pietro Massignan,[2,4,7] and Lorenzo Marrucci[1,5]

[1]Dipartimento di Fisica "Ettore Pancini", Università degli Studi di Napoli Federico II, Complesso Universitario di Monte Sant'Angelo, Via Cintia, 80126 Napoli, Italy
[2]ICFO–Institut de Ciencies Fotoniques, The Barcelona Institute of Science and Technology, 08860 Castelldefels (Barcelona), Spain
[3]ICREA–Institució Catalana de Recerca i Estudis Avançats, Pg. Lluis Companys 23, 08010 Barcelona, Spain
[4]Departament de Física, Universitat Politècnica de Catalunya, Campus Nord B4-B5, 08034 Barcelona, Spain
[5]CNR-ISASI, Institute of Applied Science and Intelligent Systems, Via Campi Flegrei 34, 80078 Pozzuoli (NA), Italy
[6]e-mail: alexandre.dauphin@icfo.eu
[7]e-mail: pietro.massignan@upc.edu
[8]e-mail: filippo.cardano2@unina.it

Received 17 April 2019; revised 25 October 2019; accepted 10 December 2019 (Doc. ID 365028); published 23 January 2020

Quantum walks are powerful tools for quantum applications and for designing topological systems. Although they are simulated in a variety of platforms, genuine two-dimensional realizations are still challenging. Here we present an innovative approach to the photonic simulation of a quantum walk in two dimensions, where walker positions are encoded in the transverse-wavevector component of a single light beam. The desired dynamics is obtained by means of a sequence of liquid-crystal devices, which apply polarization-dependent transverse "kicks" to the photons in the beam. We engineer our quantum walk so that it realizes a periodically driven Chern insulator, and we probe its topological features by detecting the anomalous displacement of the photonic wavepacket under the effect of a constant force. Our compact, versatile platform offers exciting prospects for the photonic simulation of two-dimensional quantum dynamics and topological systems. © 2020 Optical Society of America under the terms of the OSA Open Access Publishing Agreement

https://doi.org/10.1364/OPTICA.365028

1. INTRODUCTION

Quantum walks (QWs) are the deterministic quantum analogues of classical random walks and describe particles (walkers) whose discrete dynamics is conditioned by the instantaneous configuration of their spin-like degree of freedom (the coin) [1]. QWs were originally introduced as versatile candidates for implementing quantum search algorithms and universal quantum computation [2,3], and have been used to model energy transport in photosynthetic processes [4]. These systems bear close analogies with electrons in periodic potentials, and it was shown that QWs can host all possible symmetry-protected topological phases displayed by noninteracting fermions in one or two spatial dimensions (1D or 2D) [5]. Practical implementations of quantum walks have been demonstrated, for instance, with ultracold atoms in optical lattices [6–9], superconducting circuits [10], and photonic systems [11–16].

In optical architectures, the lattice coordinates have been encoded in different degrees of freedom of light, such as the arrival time of a pulse at a detector [14,17,18], the optical path of the beam [11–13,19,20], or the orbital angular momentum [15], while the coin is typically encoded in the polarization degree of freedom or in the entrance port of beam splitters. In a remarkable series of experiments, QWs proved instrumental in studying the evolution of correlated photons [12,13], the effects of decoherence [11,17] and interactions [14], Anderson localization [21], quantum transport in the presence of disorder [22], and topological phenomena in Floquet systems [10,19,23–27]. An excellent review of the state of the art on topological photonics and artificial gauge fields in quantum simulators is given in Refs. [28,29] and [30], respectively. Despite being so fruitful, experimental research on QWs has been almost entirely focused on 1D systems. Few exceptions are the studies presented in Refs. [14,18,31,32], where a 2D walk was cleverly simulated by folding a 2D lattice in a 1D chain, and in Ref. [33], where path and OAM encoding were combined. Very recently, a continuous-time walk has been realized in a 2D array of coupled waveguides [34,35].

Here, we report a novel approach to the photonic simulation of quantum dynamics on 2D discrete lattices, based on the encoding of the individual sites in the transverse wavevector (or photon momentum), which is an inherently 2D degree of freedom. In our specific case, we simulate a QW process. Unlike the common approach of using distinct optical paths (as in parallel waveguides),

in our system the photonic evolution takes place within a single light beam that acquires a complex internal structure as it propagates. The core of our photonic QW simulator is a stack of closely spaced liquid-crystal (LC) devices, conceptually similar to standard q-plates [36,37]. We present a proof-of-principle demonstration of our platform by generating up to five steps of a 2D QW, with both localized and extended initial inputs [18,38,39].

We design the unitary evolution of our QW so that it realizes a periodically driven (Floquet) Chern insulator. To characterize this system, we first analyze the energy dispersion of one of the bands of the effective Hamiltonian by tracking the free displacement of a wavepacket. Then we probe the Berry curvature of the band by repeating the tracking under the action of a constant force that is simulated by means of simple translations of specific plates. Upon sampling uniformly across the whole band, the average transverse displacement provides us a straightforward and accurate measurement of the Chern number of that band.

2. RESULTS AND DISCUSSION

A. Quantum Walks in the Transverse Wavevector of Light

A discrete-time QW on a square lattice in 2D results from the repeated action of a unitary operator U on a quantum system, the walker, and its internal spin-like degree of freedom, the coin [40]. After t discrete steps, a given initial state $|\Psi_0\rangle$ evolves according to $|\Psi(t)\rangle = U^t|\Psi_0\rangle$. The step operator U typically includes a spin rotation W, and discrete displacements of the walker along the directions x and y, generated by spin-dependent translation operators T_x and T_y. In the simplest case, the Hilbert space of the coin has dimension two [5,18]. In our photonic QW implementation, we encode the coin into light polarization. For definiteness, we use left and right circular polarizations ($|L\rangle$, $|R\rangle$) as the basis states (with handedness defined from the point of view of the receiver), like in our earlier realization of a QW with twisted light [15].

The main novelty of the setup considered here lies in encoding the discrete dimensionless coordinate of the walker $\mathbf{m} = (m_x, m_y)$ on a 2D square lattice in the transverse momentum of light. In particular, we use Gaussian modes whose mean transverse wavevector assumes the discrete values $\mathbf{k}_\perp = \Delta k_\perp \mathbf{m}$. The lattice constant $\Delta k_\perp$ is taken to be much smaller than the longitudinal wavevector component $k_z \approx 2\pi/\lambda$ (where λ is the wavelength of the light), so that these modes propagate along a direction that is only slightly tilted with respect to the z axis. More explicitly, a generic light mode in our setup reads as follows:

$$|\mathbf{m}, \phi\rangle = A(x, y, z)e^{i[\Delta k_\perp (m_x x + m_y y) + k_z z]} \otimes |\phi\rangle, \qquad (1)$$

where $A(x, y, z)$ is a Gaussian envelope with large beam radius w_0 in the transverse xy plane and $|\phi\rangle$ denotes the polarization state [see Sec. S1of Supplement 1 for more details]. Accordingly, arbitrary superpositions of these modes still form a single optical beam, traveling approximately along the z axis. Only in the far field, or equivalently in the focal plane of a lens, these modes become spatially separated, and their relative distribution can be easily readout [see Figs. 1(a) and 1(b)]. The parameters w_0 and $\Delta k_\perp$ are chosen so that these modes almost perfectly overlap spatially while propagating in the whole QW apparatus (as long as $|m_x|$ and $|m_y|$ are not too large) and have negligible crosstalk in the lens focal plane.

The QW dynamics is implemented with the apparatus depicted schematically in Fig. 1(a) and described in greater detail in Sec. S2 of Supplement 1. A collimated Gaussian laser beam passes through a sequence of closely spaced LC plates, which realize both walker-translation and coin-rotation operators. At the exit of the walk, a

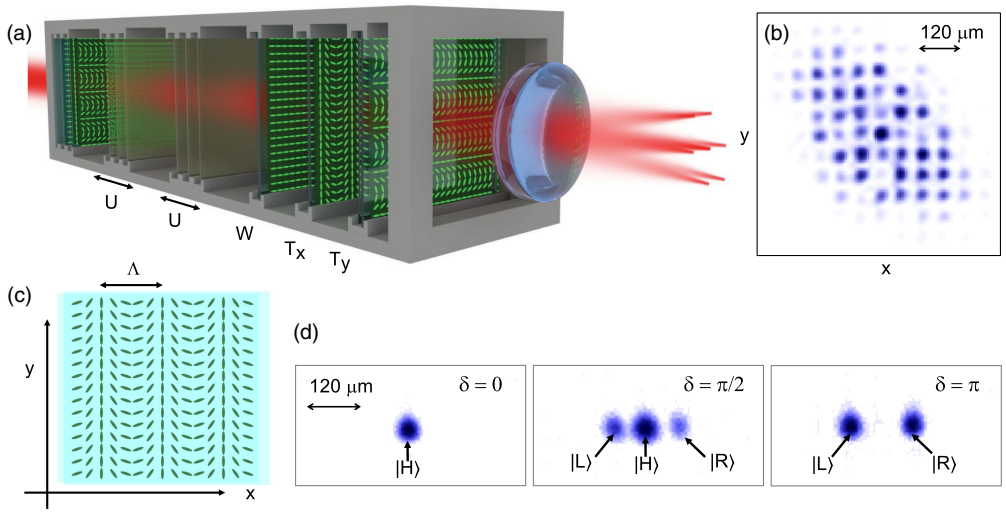

Fig. 1. Experimental concept and apparatus. (a) A collimated beam crosses a sequence of liquid-crystal (LC) devices. Different LC patterns implement coin rotations (W) and spin-dependent walker discrete translations (T_x and T_y). Each evolution step $U = T_y T_x W$ is realized with three LC devices. The walker position is encoded in the transverse momentum of photons, so that walker steps physically correspond to transverse kicks that tilt slightly the photon propagation direction. The transverse diffraction of light remains negligible across the whole setup, and the entire evolution effectively occurs in a single beam. At the exit of the walk, a lens (with focal distance equal to 50 cm) Fourier-transforms transverse momentum into position, allowing us to resolve and measure individual modes. (b) The recorded intensity pattern is a regular grid of small Gaussian spots, whose intensities are proportional to the walker's spatial probability distribution. We set the modes beam radius to $w_0 = 5$ mm, which corresponds to a spot size of $\simeq 20$ μm (radius) on the camera plane. (c) LC optic-axis pattern for a g-plate that realizes a T_x operator. The spatial period Λ fixes the transverse momentum lattice spacing $\Delta k_\perp = 2\pi/\Lambda$. We use $\Lambda = 5$ mm, so that $\Delta k_\perp = 1.26$ mm^{-1}, corresponding to a spacing between spots of $\simeq 63$ μm on the camera. (d) Action of a single g-plate T_x on a linearly polarized beam $|\Psi_0\rangle = |0, 0, H\rangle$, where $|H\rangle = (|L\rangle + |R\rangle)/\sqrt{2}$, for three different values of δ.

camera placed in the focal plane of a lens reads out the field intensity, providing the coordinates distribution of the walker [as in Fig. 1(b); see also Sec. S3 of Supplement 1]. If needed, the polarization components also may be straightforwardly read out (see Fig. S2 of Supplement 1).

The elements yielding the QW dynamics are optical devices consisting of thin layers of LC sandwiched between glass plates. The local orientation $\alpha(x, y)$ of the LC optic axis in the plane of the plate can follow arbitrary patterns, imprinted during the fabrication by a photo-alignment technique. The birefringent optical retardation δ of the LC may instead be controlled dynamically through an external electric field [37,41]. In the basis of circular polarizations $|L\rangle = (1, 0)^T$ and $|R\rangle = (0, 1)^T$, these plates act as follows:

$$L_\delta(x, y) \equiv \begin{pmatrix} \cos(\delta/2) & i\sin(\delta/2)e^{-2i\alpha(x,y)} \\ i\sin(\delta/2)e^{2i\alpha(x,y)} & \cos(\delta/2) \end{pmatrix}. \quad (2)$$

Such plates give rise to coin rotations or walker translations, depending on the optic axis pattern. For example, a spin-dependent translation operator in the x direction is obtained when the local orientation α increases linearly along x:

$$\alpha(x, y) = \pi x/\Lambda + \alpha_0, \quad (3)$$

where Λ is the spatial periodicity of the angular pattern and α_0 is a constant [see Fig. 1(c)]. This patterned birefringent structure is also known as a "polarization grating," and hence we refer here to these devices as "g-plates" (as opposed to the q-plates used in our previous works, which have azimuthally varying patterns [37]). By inserting Eq. (3) in Eq. (2), one gets the action of a g-plate:

$$T_x \equiv \begin{pmatrix} \cos(\delta/2) & i\sin(\delta/2)e^{-2i\alpha_0}\hat{t}_x \\ i\sin(\delta/2)e^{2i\alpha_0}\hat{t}_x^\dagger & \cos(\delta/2) \end{pmatrix}, \quad (4)$$

where $\hat{t}_x$ and $\hat{t}_x^\dagger$ are the (spin-independent) left and right translation operators along x, acting, respectively, as $\hat{t}_x|m_x, m_y, \phi\rangle = |m_x - 1, m_y, \phi\rangle$ and $\hat{t}_x^\dagger|m_x, m_y, \phi\rangle = |m_x + 1, m_y, \phi\rangle$. The spatial periodicity Λ of the LC pattern controls the momentum lattice spacing $\Delta k_\perp = 2\pi/\Lambda$. It is sufficient to set $\Lambda \sim w_0$ to avoid mode crosstalk. The action of a single g-plate T_x is shown in Fig. 1(d). The T_y operator is implemented analogously, imposing a gradient of the LC angle α along y. Finally, the spin rotations W are realized with uniform LC plates acting as standard quarter-wave plates, that is with constant $\alpha = 0$ and $\delta = \pi/2$. By using these values in Eq. (2), we get that in the basis of circular polarizations this operator acts as

$$W = \frac{1}{\sqrt{2}}\begin{pmatrix} 1 & i \\ i & 1 \end{pmatrix}. \quad (5)$$

B. Engineering a 2D Topological Quantum Walk

Among possible protocols obtained by combining our plates, we considered the QW generated by the unit step operator

$$U = T_y\, T_x\, W, \quad (6)$$

with T_x and T_y tuned at the same value of δ. We implemented five complete steps of this QW, which represents a generalization of the alternated protocol described in Refs. [18,38]. In particular, it realizes a periodically driven Chern insulator, exhibiting different topological phases according to the value of the parameter δ, as we discuss in detail below.

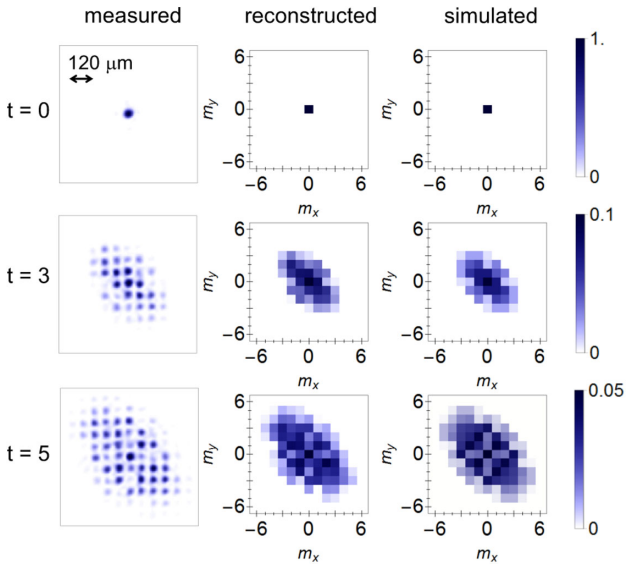

Fig. 2. 2D quantum walk on a square lattice. Spatial probability distributions for a quantum walk with initial condition $|0, 0, H\rangle$ and optical retardation $\delta = \pi/2$. From top to bottom, we display results after 0, 3, and 5 evolution steps. Datapoints are averages of four independent measures.

We start with a localized walker state $|\mathbf{m} = (0, 0), \phi\rangle$, which physically corresponds to a wide input Gaussian beam with radius $w_0 = 5$ mm, propagating along the z direction. In Fig. 2 we show representative data for $\delta = \pi/2$ and a linearly polarized input. The walker distribution remains concentrated along the diagonal $m_x = -m_y$ during the whole evolution, as a consequence of the absence of coin rotation operations between every action of T_x and T_y. All data show an excellent agreement with numerical simulations. A quantitative comparison is provided by computing the similarity $S = (\sum_{\mathbf{m}} \sqrt{P_e P_s})^2/(\sum_{\mathbf{m}} P_e \sum_{\mathbf{m}} P_s)$ between simulated (P_s) and experimental (P_e) distributions. For the data shown in Fig. 2, we have $S = (98.2 \pm 0.5)\%$, $(98.0 \pm 0.3)\%$, $(98.0 \pm 0.2)\%$ for the distributions at $t = 0$, 3, 5, respectively. The uncertainties on these values are the standard errors of the mean, obtained by repeating each experiment four times. Distributions obtained for other choices of the coin input state are reported in Figs. S5, S6 in Supplement 1.

C. Quasi-Momentum, Quasi-Energy Bands and Group Velocity

A QW can be regarded as the stroboscopic evolution generated by the (dimensionless) effective Floquet Hamiltonian $H_{\text{eff}} \equiv i \ln U$. The eigenvalues of H_{eff} are therefore defined only up to integer multiples of 2π, and are termed quasi-energies. Both U and H_{eff} admit a convenient representation in the reciprocal space $\mathbf{q}$ associated with the coordinate $\mathbf{m}$ of the walker. As discussed above, the dimensionless coordinate $\mathbf{m} = \mathbf{k}_\perp/\Delta k_\perp$ is encoded in our setup in the transverse momentum $\mathbf{k}_\perp$ of the propagating beam. As such, its conjugate variable corresponds physically to the position vector $\mathbf{r}_\perp$ in the xy transverse plane. We introduce therefore the dimensionless quasi-momentum $\mathbf{q} = -2\pi\mathbf{r}_\perp/\Lambda$, belonging to the square Brillouin zone $[-\pi, \pi]^2$, as the conjugate variable to the walker

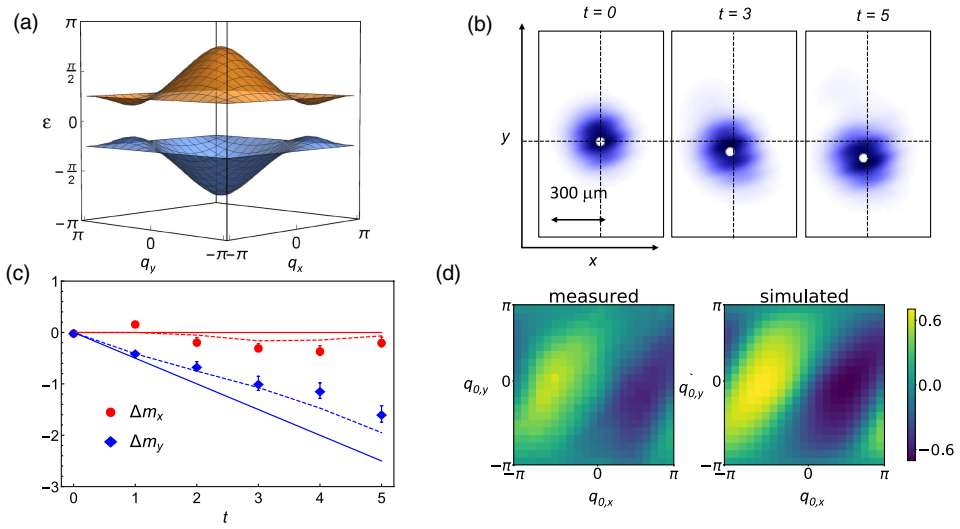

Fig. 3. Detection of the group velocity at $\delta = \pi/2$. (a) Quasi-energy spectrum of the effective Hamiltonian H_{eff}. (b) Light intensity distribution measured for a wavepacket with $\mathbf{q}_0 = (\pi/2, \pi)$ in the upper band, where the expected group velocity is $\mathbf{v}^{(+)} = (0, -0.5)$. The white marker indicates the center of mass of the wavepacket. The radius w_g of the input beam is (0.62 ± 0.02) mm. In the camera plane, we measure a beam diameter of (0.32 ± 0.01) mm, corresponding to ≈ 5 lattice sites. (c) Displacement of the wavepacket center of mass, extracted from images as in panel (b). Experimental results (datapoints) are compared to semiclassical predictions of uniform motion (straight continuous lines) and to complete numerical simulations (dashed lines). Statistical uncertainties include estimated misalignment effects, as discussed in the main text. (d) Experimental mapping of the upper band's group velocity $\mathbf{v}^{(+)}$ along x across the whole Brillouin zone, compared to a complete numerical simulation. Each datapoint is obtained from a linear fit of the center-of-mass displacement of a Gaussian wavepacket in five steps.

position $\mathbf{m}$. The negative sign in the definition of $\mathbf{q}$ provides the standard representation for plane waves $\langle \mathbf{m}|\mathbf{q}\rangle \propto e^{i\mathbf{m}\cdot\mathbf{q}}$. In the space of quasi-momenta the effective Hamiltonian assumes the diagonal form $H_{\text{eff}}(\mathbf{q}) = \varepsilon(\mathbf{q})\mathbf{n}(\mathbf{q})\cdot\sigma$. Here $\mathbf{n}(\mathbf{q})$ is a unit vector, $\sigma = (\sigma_x, \sigma_y, \sigma_z)$ represents the three Pauli matrices, and $\pm\varepsilon(\mathbf{q})$ yields the quasi-energies of two bands [as shown in Fig. 3(a)]. In the following, we will denote the complete eigenstates of the system by $|\mathbf{q}, \phi_\pm(\mathbf{q})\rangle$, where $\pm$ refers to the upper/lower band. Let us note here that, although the operator U is obtained by cascading independent displacements along the x and y axes, the overall evolution is nonseparable; that is, the effective Hamiltonian cannot be expressed as the sum of two contributions depending on a single spatial coordinate. This can be seen clearly in the expression of the quasi-energy dispersion, which is given by the following relation:

$$\cos\,\varepsilon = \frac{1}{\sqrt{2}}\Big(\cos^2(\delta/2) - \cos(\delta/2)\sin(\delta/2) \times \big(\cos(q_x) + \cos(q_y)\big) - \sin^2(\delta/2)\cos(q_x - q_y)\Big). \quad (7)$$

The complete expression of the Hamiltonian is provided in Sec. S4 of the SM.

In our experiment, we can directly explore the band structure of the system by observing the propagation of walker wavepackets $|\Psi_g(\mathbf{q}_0, \pm)\rangle$ that are sharply peaked around a given quasi-momentum $\mathbf{q}_0$ and belong to the upper/lower band. These wavepackets are physically generated as narrow Gaussian light beams (with beam radius $w_g \ll \Lambda$) propagating along the direction z, centered around a specific transverse position $\mathbf{r}_{\perp 0} = -\mathbf{q}_0\Lambda/(2\pi)$ at the input port of the QW, and with polarization $|\phi_\pm(\mathbf{q}_0)\rangle$ (see Sec. S1 of Supplement 1 for further instructions for preparing these states). In the experiment, the choice of transverse position $\mathbf{r}_{\perp 0}$ is easily controlled by translating the whole QW setup (which is mounted on a single motorized mechanical holder) relative to the input laser beam. Having narrow Gaussian envelopes in the conjugate space $\mathbf{q}$, these wavepackets are relatively broad Gaussians in the space of walker coordinates $\mathbf{m}$. They are (approximate) eigenstates of the system and therefore preserve their shape during propagation. Their center of mass $\langle\mathbf{m}\rangle_{\Psi_g}$ obeys a dynamics that semiclassically is governed by the group velocity $\mathbf{v}^{(\pm)}(\mathbf{q}_0) = \pm\nabla_{\mathbf{q}}\varepsilon(\mathbf{q})|_{\mathbf{q}=\mathbf{q}_0}$ [15], as shown for instance in Fig. 3(b). To measure experimentally the group velocity $\mathbf{v}^{(\pm)}(\mathbf{q}_0)$ we inject a wavepacket $|\Psi_g(\mathbf{q}_0, \pm)\rangle$ in our QW, we detect its average displacement $\Delta\mathbf{m}$ as a function of time-step t, and finally we perform a linear best fit on the displacements versus time [see Fig. 3(c)]. Figure 3(d) shows a complete mapping of the x component of the upper band's velocity $\mathbf{v}^{(+)}$ for $\delta = \pi/2$. Correspondingly measured values of the y component of $\mathbf{v}^{(+)}$ are reported in Fig. S7 of Supplement 1. A systematic error that can affect our setup is the possible misalignment of g-plates in both x and y directions. Our present platform permits to adjust only their position along x. As such, we can estimate the associated standard error by repeating the experiment after realigning the plates. It is not possible, however, to repeat the same procedure for the perpendicular direction. In this case, after measuring the effective displacements of the T_y plates, which are determined by fabrication imperfections, we perform a Monte Carlo simulation of the propagation of our wavepacket, and we estimate the standard deviation of the final center of the mass position. The two errors are finally combined by adding their variances to obtain the error bars in Figs. 3(c), 4(b), and 4(c).

D. Measurement of the Chern Number Through the Anomalous Velocity

The energy bands of the effective Hamiltonian generally possess nonzero Berry curvature. For a 2×2 Hamiltonian like ours, the

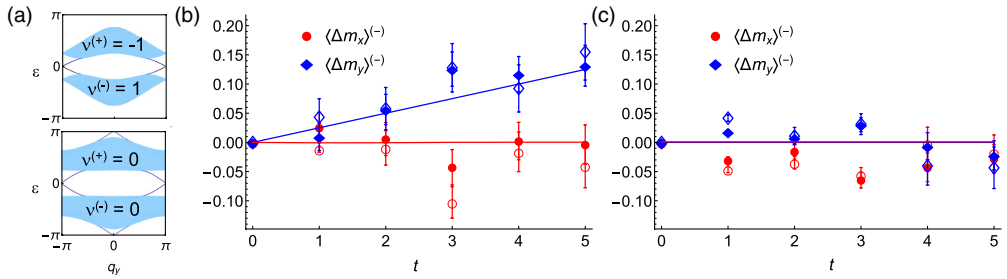

Fig. 4. Anomalous displacement for trivial and nontrivial Chern bands. (a) Quasi-energy spectra computed on a cylinder open along x for $\delta = \pi/2$ (top) and $\delta = 7\pi/8$ (bottom), showing the Chern numbers ν of the various bands. In our Floquet system, edge states (shown as darker lines inside the gaps) may be present even if all bands have vanishing Chern numbers. (b) Center-of-mass average displacement $\langle \Delta m_x \rangle^{(-)}(t)$ and $\langle \Delta m_y \rangle^{(-)}(t)$ measured for $\delta = \pi/2$ in the lower band. Empty markers show results from the simple protocol U, while solid symbols show the improved results obtained by combining protocol U with its inverse U^{-1}. Straight lines correspond to the theoretical results dictated by the semiclassical equations of motion, predicting an anomalous displacement proportional to the band Chern number. (c) Center of mass displacements measured with $\delta = 7\,\pi/8$. Meaning of all symbols and lines as in panel (b). Statistical uncertainties include estimated misalignment effects, as discussed in the main text.

latter may be written as [42]

$$\Omega_{xy}^{(\pm)}(\mathbf{q}) = \pm \frac{1}{2}\mathbf{n}(\mathbf{q}) \cdot \left[\frac{\partial \mathbf{n}}{\partial q_x} \times \frac{\partial \mathbf{n}}{\partial q_y} \right]. \tag{8}$$

The integral of the Berry curvature over the whole Brillouin zone (BZ) gives the Chern number:

$$\nu^{(\pm)} = \int_{\mathrm{BZ}} \frac{\mathrm{d}^2\mathbf{q}}{2\pi} \Omega_{xy}^{(\pm)}(\mathbf{q}). \tag{9}$$

The Chern number $\nu^{(\pm)}$ of our QW depends on the optical retardation of our plates. By tuning δ, we can thus switch from a trivial to a topological Chern insulator, as shown for example in Fig. 4(a). Our QW is a Floquet evolution, and as such its complete topological classification is not based on the Chern number only but involves a more complex invariant introduced in Ref. [43]. Such classification is discussed in detail in Sec. S5 of the SM.

When a constant unidirectional force is acting on the system, the Berry curvature contributes to the wave-packet displacement in a direction orthogonal to the force (as in the quantum Hall effect). Let us for definiteness consider a force F_x acting along x. Within the adiabatic approximation, the semiclassical equations of motion predict that a wavepacket $|\Psi_g(\mathbf{q}_0, \pm)\rangle$ will experience after a time t a transverse displacement along y given by [44,45]

$$\Delta m_y = \int_0^t \mathrm{d}\tau \left[v_y^{(\pm)}(\mathbf{q}_\tau) + F_x \Omega_{xy}^{(\pm)}(\mathbf{q}_\tau) \right], \tag{10}$$

with $\mathbf{q}_\tau = (q_{0,x} + F_x\tau, q_{0,y})$. The contribution to the velocity coming from the Berry curvature is called anomalous velocity. This result is derived in the adiabatic regime, where the (dimensionless) force is much smaller than the bandgaps of the effective energy, so that interband transitions can be neglected. When we consider the overall transverse displacement of a filled band, namely when we integrate Eq. (10) over the whole Brillouin zone, the group-velocity term averages to zero, while the anomalous contributions add up to the band's Chern number [45,46] (see Sec. S4 of Supplement 1 for a detailed derivation of this result):

$$\langle \Delta m_y \rangle^{(\pm)} \approx \frac{F_x \nu^{(\pm)}}{2\pi} t. \tag{11}$$

As shown in Eq. (10), implementing a constant force in our setup requires a linear shift in time of the quasi-momentum component q_x. This degree of freedom corresponds to the x coordinate in real space. Hence, we impose at each step a quasi-momentum variation by introducing a transverse spatial displacement of the light beam between each plate. Actually, rather than displacing the beam, it is equivalent (and much simpler) to displace the reference system and the setup in the opposite direction. More specifically, we shift the g-plate acting at time-step t along the x axis by an amount $\Delta x_t = t F_x \Lambda/(2\pi)$ (see Sec. S4 in Supplement 1 for further details). Then, we sum up the measured displacements Δm_y obtained for 11×11 distinct wave-packets $|\Psi_g(\mathbf{q}_0, -)\rangle$, providing a homogeneous sampling of the lower band across the whole Brillouin zone and realizing a good approximation of the continuous integral yielding $\langle \Delta m_y \rangle^{(-)}$. Figure 4(b) shows the mean displacement of wavepackets prepared in the lowest energy band for a QW with $\delta = \pi/2$, corresponding to Chern number $\nu^{(-)} = 1$. The energy bandgap ≈ 1 [see Fig. 4(a)] is sufficiently larger than the applied force $F_x = \pi/20$, thereby ensuring the validity of the adiabatic approximation. Experimental data (empty markers) are compared to the overall band displacement predicted by the semiclassical theory within adiabatic regime (continuous lines), namely $\langle \Delta m_y(t) \rangle^{(-)} = t\nu^{(-)} F_x/(2\pi)$, $\langle \Delta m_x(t) \rangle^{(-)} = 0$. While $\langle \Delta m_y \rangle^{(-)}$ follows the expected curve quite reasonably, the overall $\langle \Delta m_x \rangle^{(-)}$ is found to be not negligible. These small differences can be understood by simulating the full dynamics of the wave packet, beyond the single band approximation (see Fig. S8 in Supplement 1).

To get rid of this spurious contribution, which arises mainly from residual group-velocity effects, we consider also the "inverse protocol" generated by the step operator $U^{-1} = W^{-1} T_x^{-1} T_y^{-1}$. The bands of U^{-1} have the same dispersion as the bands of U but feature opposite Chern numbers. In this way, if filling the same band, we expect to observe identical contributions from the group velocity dispersion, while the anomalous displacement should be inverted. The step operator U^{-1} can be easily implemented by swapping the T_y and W operators and changing suitably their retardation (see Sec. S4 and Fig. S2 in Supplement 1). In Fig. 4(b) we show with filled markers the difference (divided by two) of the data obtained with the protocols U and U^{-1}. This procedure reduces significantly the overall displacement along x, while in the y direction we observe a very nice agreement between our data and the semiclassical predictions. The measured value of the Chern number is $\nu^{(-)} = 1.19 \pm 0.13$, consistent with the theoretical

value of 1 (errors are given at one standard deviation). A similar behavior is also observed for larger values of the force, as shown in Fig. S9 in Supplement 1. In Fig. 4(c), we replicate the same experiment for a QW with $\delta = 7\pi/8$, when the Chern numbers are zero, even though the presence of edge states witnesses nontrivial topology [43] (see also Sec. S5 of Supplement 1). In agreement with the prediction of vanishing anomalous displacement, the average wavepacket motion in both directions is observed to be negligible, yielding a Chern number $\nu^{(-)} = 0.10 \pm 0.15$.

3. CONCLUSION

In this work we have experimentally demonstrated a conceptually new scheme for the realization of a 2D discrete-time QW, that relies on encoding the walker and the coin systems into the transverse momentum of photons and in their polarization, respectively. The coin rotation and shift operators are implemented by suitably engineered LC plates, whose number scales linearly with the number of time-steps. They are arranged in a compact setup, in which multiple degrees of freedom can be controlled dynamically, such as the plates' optical retardation δ or their transverse position, allowing one to study several QW architectures. If needed, different LC patterns could be written onto the plates, yielding different types of quantum dynamics. The platform accurately simulates the dynamics dictated by the QW protocols that we tested, as witnessed by the good agreement between measured distributions and numerical results. We investigated 2D walks of both localized and extended inputs, with and without an external force. The 2D protocol we presented here simulates a Floquet Chern insulator. We probed the associated topological features by preparing wave-packets that well approximate the eigenstates of the QW Floquet Hamiltonian and detecting their average anomalous displacement arising when a constant force is applied to the system.

The setup has been designed to minimize the decoherence effects caused by light diffraction and walkoff phase delays occurring when the walker follows different paths (see Sec. S7 of Supplement 1). There is no fundamental limitation to scaling up our setup to a much larger number of steps. Reflection losses at each LC plate ($\simeq 15\%$), representing the main current limitation to the setup efficiency, could be largely reduced to the level of 1%–2% by applying a standard antireflection coating. As such, while our experiment is carried out in a classical-wave regime, the proposed setup is perfectly suitable for single-photon quantum experiments, similarly to what was already demonstrated in Ref. [15]. These represent one of the most appealing future prospects for our system, particularly in view of the very large number of input and output modes that can be easily addressed.

The demonstration of a new platform for 2D QWs opens new avenues for the experimental study of the rich quantum dynamics in two dimensions. In prospect, diverse directions could be investigated with our platform, such as the realization of 2D lattices with more complex topologies (for example, hexagonal), or experiments in the multiphoton regime, for instance in the context of QW applications to Boson sampling. Direct access to both walker position and quasi-momentum could be exploited to study complex dynamics in the regime of spatial disorder. By combining topology and our dynamical control of the system parameters, we could investigate dynamical quantum phase transitions in QWs [47–49]. Finally, by introducing losses for specific polarization states, this platform could be used to investigate topological features of 2D non-Hermitian systems [50–53].

Funding. H2020 European Research Council (694683); FP7 Ideas: European Research Council (339106); H2020 Future and Emerging Technologies (641122); Fundación Cellex; Ministerio de Economía y Competitividad (SEV-2015-0522, FIS2016-79508-P, SWUQM FIS2017-84114-C2-1-P); Generalitat de Catalunya (CERCA, SGR874); Ministerio de Ciencia, Innovación y Universidades (IJCI-2017-33180, Ramón y Cajal).

Acknowledgment. LM conceived the 2D photon-momentum encoding strategy. AD'E, FC, and LM designed the setup. AD'E devised the 2D QW protocol. AD'E, FC, and RB, with contributions from CE, performed the experiments and analyzed the data. MM, ADa, and PM developed the theoretical framework and devised the scheme for the anomalous displacement detection. BP, with the help of AD'E and FC, fabricated the *g*-plates. AD'E, FC, RB, ADa, MM, PM, and LM wrote the manuscript. LM and ML supervised the project. All authors discussed the results and contributed to refining the paper.

See Supplement 1 for supporting content.

[†]These authors contributed equally to this work.

REFERENCES

1. S. E. Venegas-Andraca, "Quantum walks: a comprehensive review," Quantum Inf. Process. **11**, 1015–1106 (2012).
2. N. Shenvi, J. Kempe, and K. B. Whaley, "Quantum random-walk search algorithm," Phys. Rev. A **67**, 052307 (2003).
3. A. M. Childs, "Universal computation by quantum walk," Phys. Rev. Lett. **102**, 180501 (2009).
4. M. Mohseni, P. Rebentrost, S. Lloyd, and A. Aspuru-Guzik, "Environment-assisted quantum walks in photosynthetic energy transfer," J. Chem. Phys. **129**, 174106 (2008).
5. T. Kitagawa, M. S. Rudner, E. Berg, and E. Demler, "Exploring topological phases with quantum walks," Phys. Rev. A **82**, 033429 (2010).
6. M. Karski, L. Forster, J.-M. Choi, A. Steffen, W. Alt, D. Meschede, and A. Widera, "Quantum walk in position space with single optically trapped atoms," Science **325**, 174–177 (2009).
7. M. Genske, W. Alt, A. Steffen, A. H. Werner, R. F. Werner, D. Meschede, and A. Alberti, "Electric quantum walks with individual atoms," Phys. Rev. Lett. **110**, 190601 (2013).
8. P. M. Preiss, R. Ma, M. E. Tai, A. Lukin, M. Rispoli, P. Zupancic, Y. Lahini, R. Islam, and M. Greiner, "Strongly correlated quantum walks in optical lattices," Science **347**, 1229–1233 (2015).
9. S. Dadras, A. Gresch, C. Groiseau, S. Wimberger, and G. S. Summy, "Quantum walk in momentum space with a Bose-Einstein condensate," Phys. Rev. Lett. **121**, 070402 (2018).
10. E. Flurin, V. V. Ramasesh, S. Hacohen-Gourgy, L. S. Martin, N. Y. Yao, and I. Siddiqi, "Observing topological invariants using quantum walks in superconducting circuits," Phys. Rev. X **7**, 031023 (2017).
11. M. A. Broome, A. Fedrizzi, B. P. Lanyon, I. Kassal, A. Aspuru-Guzik, and A. G. White, "Discrete single-photon quantum walks with tunable decoherence," Phys. Rev. Lett. **104**, 153602 (2010).
12. A. Peruzzo, M. Lobino, J. C. F. Matthews, N. Matsuda, A. Politi, K. Poulios, X.-Q. Zhou, Y. Lahini, N. Ismail, K. Worhoff, Y. Bromberg, Y. Silberberg, M. G. Thompson, and J. L. O'Brien, "Quantum walks of correlated photons," Science **329**, 1500–1503 (2010).
13. L. Sansoni, F. Sciarrino, G. Vallone, P. Mataloni, A. Crespi, R. Ramponi, and R. Osellame, "Two-particle Bosonic-Fermionic quantum walk via integrated photonics," Phys. Rev. Lett. **108**, 010502 (2012).
14. A. Schreiber, A. Gabris, P. P. Rohde, K. Laiho, M. Stefanak, V. Potocek, C. Hamilton, I. Jex, and C. Silberhorn, "A 2D quantum walk simulation of two-particle dynamics," Science **336**, 55–58 (2012).
15. F. Cardano, F. Massa, H. Qassim, E. Karimi, S. Slussarenko, D. Paparo, C. de Lisio, F. Sciarrino, E. Santamato, R. W. Boyd, and L. Marrucci,

"Quantum walks and wavepacket dynamics on a lattice with twisted photons," Sci. Adv. **1**, e1500087 (2015).
16. H. Defienne, M. Barbieri, I. A. Walmsley, B. J. Smith, and S. Gigan, "Two-photon quantum walk in a multimode fiber," Sci. Adv. **2**, e1501054 (2016).
17. A. Schreiber, K. N. Cassemiro, V. Potoček, A. Gábris, I. Jex, and C. Silberhorn, "Decoherence and disorder in quantum walks: from ballistic spread to localization," Phys. Rev. Lett. **106**, 180403 (2011).
18. Y.-C. Jeong, C. Di Franco, H.-T. Lim, M. Kim, and Y.-H. Kim, "Experimental realization of a delayed-choice quantum walk," Nat. Commun. **4**, 2471 (2013).
19. T. Kitagawa, M. A. Broome, A. Fedrizzi, M. S. Rudner, E. Berg, I. Kassal, A. Aspuru-Guzik, E. Demler, and A. G. White, "Observation of topologically protected bound states in photonic quantum walks," Nat. Commun. **3**, 882 (2012).
20. K. Poulios, R. Keil, D. Fry, J. D. A. Meinecke, J. C. F. Matthews, A. Politi, M. Lobino, M. Gräfe, M. Heinrich, S. Nolte, A. Szameit, and J. L. O'Brien, "Quantum walks of correlated photon pairs in two-dimensional waveguide arrays," Phys. Rev. Lett. **112**, 143604 (2014).
21. A. Crespi, R. Osellame, R. Ramponi, V. Giovannetti, R. Fazio, L. Sansoni, F. De Nicola, F. Sciarrino, and P. Mataloni, "Anderson localization of entangled photons in an integrated quantum walk," Nat. Photonics **7**, 322–328 (2013).
22. N. C. Harris, G. R. Steinbrecher, M. Prabhu, Y. Lahini, J. Mower, D. Bunandar, C. Chen, F. N. C. Wong, T. Baehr-Jones, M. Hochberg, S. Lloyd, and D. Englund, "Quantum transport simulations in a programmable nanophotonic processor," Nat. Photonics **11**, 447–452 (2017).
23. J. M. Zeuner, M. C. Rechtsman, Y. Plotnik, Y. Lumer, S. Nolte, M. S. Rudner, M. Segev, and A. Szameit, "Observation of a topological transition in the bulk of a non-Hermitian system," Phys. Rev. Lett. **115**, 040402 (2015).
24. F. Cardano, M. Maffei, F. Massa, B. Piccirillo, C. de Lisio, G. De Filippis, V. Cataudella, E. Santamato, and L. Marrucci, "Dynamical moments reveal a topological quantum transition in a photonic quantum walk," Nat. Commun. **7**, 11439 (2015).
25. F. Cardano, A. D'Errico, A. Dauphin, M. Maffei, B. Piccirillo, C. de Lisio, G. De Filippis, V. Cataudella, E. Santamato, L. Marrucci, M. Lewenstein, and P. Massignan, "Detection of Zak phases and topological invariants in a chiral quantum walk of twisted photons," Nat. Commun. **8**, 15516 (2017).
26. L. Xiao, X. Zhan, Z. H. Bian, K. K. Wang, X. Zhang, X. P. Wang, J. Li, K. Mochizuki, D. Kim, N. Kawakami, W. Yi, H. Obuse, B. C. Sanders, and P. Xue, "Observation of topological edge states in parity-time-symmetric quantum walks," Nat. Phys. **13**, 1117–1123 (2017).
27. X. Zhan, L. Xiao, Z. Bian, K. Wang, X. Qiu, B. C. Sanders, W. Yi, and P. Xue, "Detecting topological invariants in nonunitary discrete-time quantum walks," Phys. Rev. Lett. **119**, 130501 (2017).
28. A. B. Khanikaev and G. Shvets, "Two-dimensional topological photonics," Nat. Photonics **11**, 763–773 (2017).
29. T. Ozawa, H. M. Price, A. Amo, N. Goldman, M. Hafezi, L. Lu, M. C. Rechtsman, D. Schuster, J. Simon, O. Zilberberg, and I. Carusotto, "Topological photonics," Rev. Mod. Phys. **91**, 015006 (2019).
30. M. Aidelsburger, S. Nascimbene, and N. Goldman, "Artificial gauge fields in materials and engineered systems," C. R. Physique **19**, 394 (2018).
31. C. Chen, X. Ding, J. Qin, Y. He, Y.-H. Luo, M.-C. Chen, C. Liu, X.-L. Wang, W.-J. Zhang, H. Li, L.-X. You, Z. Wang, D.-W. Wang, B. C. Sanders, C.-Y. Lu, and J.-W. Pan, "Observation of topologically protected edge states in a photonic two-dimensional quantum walk," Phys. Rev. Lett. **121**, 100502 (2018).
32. H. Chalabi, S. Barik, S. Mittal, T. E. Murphy, M. Hafezi, and E. Waks, "Synthetic gauge field for two-dimensional time-multiplexed quantum random walks," Phys. Rev. Lett. **123**, 150503 (2019).
33. B. Wang, T. Chen, and X. Zhang, "Experimental observation of topologically protected bound states with vanishing Chern numbers in a two-dimensional quantum walk," Phys. Rev. Lett. **121**, 100501 (2018).
34. H. Tang, X.-F. Lin, Z. Feng, J.-Y. Chen, J. Gao, K. Sun, C.-Y. Wang, P.-C. Lai, X.-Y. Xu, Y. Wang, L.-F. Qiao, A.-L. Yang, and X.-M. Jin, "Experimental two-dimensional quantum walk on a photonic chip," Sci. Adv. **4**, eaat3174 (2018).
35. H. Tang, C. Di Franco, Z.-Y. Shi, T.-S. He, Z. Feng, J. Gao, K. Sun, Z.-M. Li, Z.-Q. Jiao, T.-Y. Wang, M. S. Kim, and X.-M. Jin, "Experimental quantum fast hitting on hexagonal graphs," Nat. Photonics **12**, 754–758 (2018).
36. L. Marrucci, C. Manzo, and D. Paparo, "Optical spin-to-orbital angular momentum conversion in inhomogeneous anisotropic media," Phys. Rev. Lett. **96**, 163905 (2006).
37. A. Rubano, F. Cardano, B. Piccirillo, and L. Marrucci, "Q-plate technology: a progress review [Invited]," J. Opt. Soc. Am. B **36**, D70–D87 (2019).
38. C. Di Franco, M. Mc Gettrick, and T. Busch, "Mimicking the probability distribution of a two-dimensional Grover walk with a single-qubit coin," Phys. Rev. Lett. **106**, 080502 (2011).
39. C. Di Franco, M. Mc Gettrick, T. Machida, and T. Busch, "Alternate two-dimensional quantum walk with a single-qubit coin," Phys. Rev. A **84**, 042337 (2011).
40. Y. Aharonov, L. Davidovich, and N. Zagury, "Quantum random walks," Phys. Rev. A **48**, 1687–1690 (1993).
41. B. Piccirillo, V. D'Ambrosio, S. Slussarenko, L. Marrucci, and E. Santamato, "Photon spin-to-orbital angular momentum conversion via an electrically tunable q-plate," Appl. Phys. Lett. **97**, 241104 (2010).
42. X.-L. Qi, T. L. Hughes, and S.-C. Zhang, "Topological field theory of time-reversal invariant insulators," Phys. Rev. B **78**, 195424 (2008).
43. M. S. Rudner, N. H. Lindner, E. Berg, and M. Levin, "Anomalous edge states and the bulk-edge correspondence for periodically driven two-dimensional systems," Phys. Rev. X **3**, 031005 (2013).
44. D. Xiao, M.-C. Chang, and Q. Niu, "Berry phase effects on electronic properties," Rev. Mod. Phys. **82**, 1959–2007 (2010).
45. H. M. Price, O. Zilberberg, T. Ozawa, I. Carusotto, and N. Goldman, "Measurement of Chern numbers through center-of-mass responses," Phys. Rev. B **93**, 245113 (2016).
46. A. Dauphin and N. Goldman, "Extracting the Chern number from the dynamics of a Fermi gas: Implementing a quantum Hall bar for cold atoms," Phys. Rev. Lett. **111**, 135302 (2013).
47. K. Wang, X. Qiu, L. Xiao, X. Zhan, Z. Bian, W. Yi, and P. Xue, "Simulating dynamic quantum phase transitions in photonic quantum walks," Phys. Rev. Lett. **122**, 020501 (2019).
48. X.-Y. Xu, Q.-Q. Wang, M. Heyl, J. C. Budich, W.-W. Pan, Z. Chen, M. Jan, K. Sun, J.-S. Xu, Y.-J. Han, C.-F. Li, and G.-C. Guo, "Measuring a dynamical topological order parameter in quantum walks," arXiv:1808.03930 (2018).
49. M. Heyl, "Dynamical quantum phase transitions: a review," Rep. Prog. Phys. **81**, 054001 (2018).
50. S. Longhi, "Parity-time symmetry meets photonics: a new twist in non-Hermitian optics," Europhys. Lett. **120**, 64001 (2017).
51. S. Yao, F. Song, and Z. Wang, "Non-Hermitian Chern bands," Phys. Rev. Lett. **121**, 136802 (2018).
52. Z. Gong, Y. Ashida, K. Kawabata, K. Takasan, S. Higashikawa, and M. Ueda, "Topological phases of non-Hermitian systems," Phys. Rev. X **8**, 031079 (2018).
53. K. Yokomizo and S. Murakami, "Non-Bloch band theory of non-Hermitian systems," Phys. Rev. Lett. **123**, 066404 (2019).

143.225.204.253 {ts '2020-01-24 03:36:51'}